

Photoproduction of e^+e^- in peripheral isobar collisions

Shuo Lin,^{1,*} Ren-Jie Wang,^{1,†} Jian-Fei Wang,^{1,‡}

Hao-Jie Xu,^{2,§} Shi Pu,^{1,¶} and Qun Wang^{1,**}

¹*Department of Modern Physics, University of Science
and Technology of China, Anhui 230026, China*

²*School of Science, Huzhou University, Huzhou, Zhejiang, 313000, China*

Abstract

We investigate the photoproduction of di-electrons in peripheral collisions of $^{96}_{44}\text{Ru} + ^{96}_{44}\text{Ru}$ and $^{96}_{40}\text{Zr} + ^{96}_{40}\text{Zr}$ at 200 GeV. With the charge and mass density distributions given by the calculation of the density functional theory, we calculate the spectra of transverse momentum, invariant mass and azimuthal angle for di-electrons at 40-80% centrality. The ratios of these spectra in Ru+Ru collisions over to Zr+Zr collisions are shown to be smaller than $(44/40)^4$ (the ratio of Z^4 for Ru and Zr) at low transverse momentum. The deviation arises from the different mass and charge density distributions in Ru and Zr. So the photoproduction of di-leptons in isobar collisions may provide a new way to probe the nuclear structure.

* linshuo@mail.ustc.edu.cn

† wrgn@mail.ustc.edu.cn

‡ wjf1996@mail.ustc.edu.cn

§ haojiexu@zjhu.edu.cn

¶ shipu@ustc.edu.cn

** qunwang@ustc.edu.cn

I. INTRODUCTION

In ultra-relativistic heavy ion collisions, extremely strong electromagnetic fields (of order 10^{15} Tesla) are generated when two colliding nuclei pass through each other [1–5]. Such strong electromagnetic fields provide an experimental platform for the study of novel quantum transport phenomena under extreme conditions, such as the chiral magnetic and separation effects [6, 7], the chiral electric separation effect [8, 9], and other nonlinear effects [10–12]. These chiral transport phenomena can be described by microscopic quantum kinetic theories [12–49] and macroscopic magnetohydrodynamics [5, 50–54], see, e.g., Refs. [45, 55–62] for recent reviews. On the other hand, it is also possible to study nonlinear effects of quantum electrodynamics (QED) in ultra-relativistic heavy ion collisions, such as light-by-light scatterings [63], matter generation directly from photons [64, 65], vacuum birefringence [64, 66–70] and Schwinger mechanism [71–74].

In recent years, the lepton pair photoproduction in peripheral and ultra-peripheral collisions has been extensively studied in both experiments and theories. To give a better understanding of experimental data [64, 75–77], besides the equivalent photon approximation (EPA) by STARlight [78], several theoretical methods have been developed, such as QED models with generalized EPA in the background field approach [65, 79–86], the method based on the factorization theorem [87–90] and the QED model with the wave-packet description of nuclei [91, 92]. Furthermore, it has been shown in Ref. [85, 89] that linearly polarized photons, similar to linearly polarized gluons [93–97], can generate the azimuthal angle modulation measured by the STAR collaboration [64]. A similar azimuthal angle asymmetry in diffractive production of pions related to elliptic gluon Wigner distribution in ultra-peripheral collisions is proposed in Ref. [98]. So the photonuclear reaction can be used to probe the properties of initial gluons [98–102].

The isobar collisions of $^{96}_{44}\text{Ru}+^{96}_{44}\text{Ru}$ and $^{96}_{40}\text{Zr}+^{96}_{40}\text{Zr}$ at the top collision energy of RHIC were originally proposed to search for the chiral magnetic effect (CME) [103]. Since Ru and Zr are isobars (with the same nucleon number but different proton numbers), the electromagnetic fields and thus the chiral magnetic effect should be different in isobar collisions at the same centrality, while the backgrounds related to collision geometry, such as the elliptic flow v_2 and charged hadron multiplicity N_{ch} , are expected to be the same. However, according to the calculation based on the energy density functional theory (DFT), there are sizable

differences in nuclear density distributions for CME backgrounds which ruin the initial premise of isobar collisions for the CME search [104, 105]. This has recently been confirmed by the isobar data of STAR collaboration [106], indicating that the structure of isobar nuclei is crucial to the baseline for the CME signal. The lepton pair photoproduction depends on the charge distributions of colliding nuclei, which may provide a further constraint on the nuclear structure parameters in isobar collisions.

In this paper, we employ the theoretical method developed in previous studies [91, 92] by some of us to investigate the lepton pair photoproduction in isobar collisions. The method is based on QED in a classical field approximation with the wave-packet description of colliding nuclei encoding the information of the polarization and transverse momentum (or impact parameter) dependence of photons in the differential cross section. It can describe the photoproduction data of lepton pairs in peripheral and ultra-peripheral collisions [64, 76, 107].

We will calculate the transverse momentum, invariant mass and azimuthal angle distributions for e^+e^- pairs at $\sqrt{s_{\text{NN}}} = 200$ GeV in Ru+Ru and Zr+Zr collisions. The Woods-Saxon parameters for isobar nuclei are obtained by the state-of-art DFT calculation through nuclear charge and mass density distributions [108]. Since the nuclear mass and charge density distributions give sizable difference in multiplicity distributions in isobar collisions, the lepton pair photoproduction is calculated with the charge density distribution, while the centrality is defined from the Glauber model with the nuclear mass density. The centrality determined from the charge density distribution will also be computed as a control. This study provides a new way of probing the nuclear structure through photoproduction of lepton pairs in isobar collisions.

The paper is organized as follows. In Sec. II, we briefly review the theoretical method [91] and introduce the parameters in the numerical calculation. In Sec. III, we present the transverse momentum, invariant mass and azimuthal angle distributions for e^+e^- at $\sqrt{s_{\text{NN}}} = 200$ GeV in Ru+Ru and Zr+Zr collisions. We study the charge and centrality dependence of the cross section in Sec. IV. We make a summary of the main result in Sec. V.

Notational convention. We use $\mathbf{P}_T^{\text{ee}} = \mathbf{k}_{1T} + \mathbf{k}_{2T}$ for the transverse momentum of the electron pair and $\mathbf{K}_T^{\text{ee}} = \frac{1}{2}(\mathbf{k}_{2T} - \mathbf{k}_{1T})$ for the difference in transverse momentum between the electron and positron. We use M_{ee} for the invariant mass of the electron pair and ϕ for

the angle between \mathbf{P}_T^{ee} and \mathbf{K}_T^{ee} . We also use $P_T^{\text{ee}} = |\mathbf{P}_T^{\text{ee}}|$ and $K_T^{\text{ee}} = |\mathbf{K}_T^{\text{ee}}|$ for the lengths of two vectors.

II. THEORETICAL METHOD AND SETUP

We will use in our calculation the method developed by some of us for lepton pair photoproduction in the classical field approximation with the wave packet description of nuclei [91, 92]. Suppose two identical nuclei A_1 and A_2 move in $\pm z$ direction with the velocity $u_{1,2}^\mu = \gamma(1, 0, 0, \pm v)$ [$\gamma = 1/\sqrt{1-v^2}$ is the Lorentz factor] respectively. Two photons from colliding nuclei produce a lepton pair as $\gamma(p_1) + \gamma(p_2) \rightarrow l(k_1) + l(k_2)$, where p_1^μ and p_2^μ are four-momenta of photons (photons are not exactly on-shell), and $k_1^\mu = (E_{k_1}, \mathbf{k}_1)$ and $k_2^\mu = (E_{k_2}, \mathbf{k}_2)$ are on-shell four-momenta leptons. The Born-level total cross section can be written into a compact form,

$$\begin{aligned} \sigma &= \frac{Z^4 e^4}{2\gamma^4 v^3} \int d^2\mathbf{b}_T d^2\mathbf{b}_{1T} d^2\mathbf{b}_{2T} \int \frac{d\omega_1 d^2\mathbf{p}_{1T}}{(2\pi)^3} \frac{d\omega_2 d^2\mathbf{p}_{2T}}{(2\pi)^3} \\ &\times \int \frac{d^2\mathbf{p}'_{1T}}{(2\pi)^2} e^{-i\mathbf{b}_{1T} \cdot (\mathbf{p}'_{1T} - \mathbf{p}_{1T})} \frac{F^*(-\bar{p}'_1)}{-\bar{p}'_1{}^2} \frac{F(-\bar{p}_1)}{-\bar{p}_1{}^2} \\ &\times \int \frac{d^2\mathbf{p}'_{2T}}{(2\pi)^2} e^{-i\mathbf{b}_{2T} \cdot (\mathbf{p}'_{2T} - \mathbf{p}_{2T})} \frac{F^*(-\bar{p}'_2)}{-\bar{p}'_2{}^2} \frac{F(-\bar{p}_2)}{-\bar{p}_2{}^2} \\ &\times \int \frac{d^3k_1}{(2\pi)^3 2E_{k_1}} \frac{d^3k_2}{(2\pi)^3 2E_{k_2}} (2\pi)^4 \delta^{(4)}(\bar{p}_1 + \bar{p}_2 - k_1 - k_2) \delta^{(2)}(\mathbf{b}_T - \mathbf{b}_{1T} + \mathbf{b}_{2T}) \\ &\times \sum_{\text{spin of } l, \bar{l}} [u_{1\mu} u_{2\nu} L^{\mu\nu}(\bar{p}_1, \bar{p}_2; k_1, k_2)] [u_{1\sigma} u_{2\rho} L^{\sigma\rho*}(\bar{p}'_1, \bar{p}'_2; k_1, k_2)], \end{aligned} \quad (1)$$

where Z is the proton number of the nuclei, \mathbf{b}_{iT} is the transverse position of the photon emission in the nucleus A_i , \mathbf{b}_T is the impact parameter of colliding nuclei, \bar{p}_i and \bar{p}'_i are photon momenta in the classical field approximation and defined as ($i = 1, 2$)

$$\bar{p}_i^\mu = \left(\omega_i, \mathbf{p}_{iT}, (-1)^{i+1} \frac{\omega_i}{v} \right), \quad \bar{p}'_i{}^\mu = \left(\omega_i, \mathbf{p}'_{iT}, (-1)^{i+1} \frac{\omega_i}{v} \right), \quad (2)$$

satisfying $\bar{p}_i \cdot u_i = \bar{p}'_i \cdot u_i = 0$, the lepton tensor $L^{\mu\nu}$ is given by

$$\begin{aligned} L^{\mu\nu}(p_1, p_2; k_1, k_2) &= -ie^2 \bar{u}(k_1) \left[\gamma^\mu \frac{\gamma \cdot (k_1 - p_1) + m}{(k_1 - p_1)^2 - m^2 + i\varepsilon} \gamma^\nu \right. \\ &\quad \left. + \gamma^\nu \frac{\gamma \cdot (p_1 - k_2) + m}{(p_1 - k_2)^2 - m^2 + i\varepsilon} \gamma^\mu \right] v(k_2), \end{aligned} \quad (3)$$

and $F(-p^2)$ is the nuclear charge form factor, Fourier transform of the nuclear charge density distribution.

Table I. Parameters for the charge and mass form factors of Ru and Zr and centralities with corresponding impact parameters. (a) The charge and mass density distributions from DFT calculation. The centralities and impact parameters are defined by the mass density distribution; (b) The centralities and impact parameters are defined by the charge density distribution determined from DFT calculation.

(a)	R_c	d_c	R_n	d_n	Centrality	40%	60%	70%	80%
Ru	5.083 fm	0.477 fm	5.093 fm	0.488 fm	Impact parameter	7.464 fm	9.143 fm	9.874 fm	10.563 fm
Zr	4.977 fm	0.492 fm	5.022 fm	0.538 fm	Impact parameter	7.615 fm	9.326 fm	10.073fm	10.780 fm
(b)	R_c	d_c	R_n	d_n	Centrality	40%	60%	70%	80%
Ru	5.083 fm	0.477 fm	R_c^{Ru}	d_c^{Ru}	Impact parameter	7.406 fm	9.070 fm	9.797 fm	10.479 fm
Zr	4.977 fm	0.492 fm	R_c^{Zr}	d_c^{Zr}	Impact parameter	7.373 fm	9.030 fm	9.754 fm	10.434 fm

The density distributions for the nuclear charge (proton) and mass (nucleon) are obtained from the state-of-art DFT calculation. Same as Ref. [108, 109], we parameterize the charge or mass density distributions with the Woods-Saxon (WS) distribution,

$$\rho_i(\mathbf{r}) \equiv \frac{C_i}{1 + \exp[(|\mathbf{r}| - R_i)/d_i]}, \quad (4)$$

by matching $\langle r \rangle$ and $\langle r^2 \rangle$. Here $i = c, n$ denotes the charge and mass density distribution respectively, and R_i, d_i, C_i are the corresponding radius, skin depth and normalization factor, respectively. In the calculation, we use the charge density distribution for the cross section in Eq. (1), so $F(-p^2)$ is the nuclear charge form factor defined as $F_c(\mathbf{k}^2) = \int d^3r e^{i\mathbf{k}\cdot\mathbf{r}} \rho_c(\mathbf{r})$. We use the mass density distribution $\rho_n(\mathbf{r})$ to determine the impact parameter \mathbf{b}_T through the centrality of collisions.

The charge and mass density distributions give sizable difference in the multiplicity and thus centrality in isobar collisions [104, 105, 110]. The WS parameters for the charge and mass density distributions and the centralities with corresponding impact parameters are listed in Tab. I. In Tab. I(a) the centralities with corresponding impact parameters are defined by the mass density distribution which has different WS parameters from the charge density distribution. We will label the numerical results in this case as “(a) DFT”. For comparison, we also use the charge density distribution as the mass density distribution to define the centrality as shown in Tab. I(b). We will label the numerical results in this case

as “(b) charge=mass”. The impact parameters and centralities are calculated by an optical Glauber model as in Ref. [111] with $\sigma_{\text{NN}} = 42$ mb at $\sqrt{s_{\text{NN}}} = 200$ GeV. We have checked that parameters used in Ref. [110] belong to the case “(b) charge=mass”. This indicates that the lepton pair photoproduction in isobar collisions can reflect the information about nuclear structure of colliding nuclei.

In principle, the deformation of isobar nuclei [106, 112] can also change the profile of classical photon fields and introduce a higher order correction to the differential cross sections. However, a systematic study of the deformation effect may require computing the differential cross section (1) with the classical photon fields on the event-by-event basis, which is challenging. Therefore, as a first attempt, we do not consider the deformation effect in the current study.

We follow STAR experiments [64, 76, 107] to set that the transverse momentum of the electron or positron is greater than 200 MeV. The rapidity range of e^+e^- pair and pseudo-rapidity range of a single electron or positron are set to $[-1, 1]$. To deal with the high dimensional integration in Eq. (1), we implement the ZMCintegral package [113, 114] (also see Ref. [115, 116] for other applications of the package).

III. TRANSVERSE MOMENTUM, INVARIANT MASS AND AZIMUTHAL ANGLE DISTRIBUTIONS

In this section, we present numerical results for transverse momentum, invariant mass and azimuthal angle distributions for e^+e^- in Ru+Ru and Zr+Zr collisions at $\sqrt{s_{\text{NN}}} = 200$ GeV. Without the difference in the nuclear structure, the ratio of the differential cross section in Ru+Ru collisions to Zr+Zr collisions at the same collision energy should only depend on the number of protons, i.e. $(44/40)^4$, as in Eq. (1). However, we will show that the difference in nuclear structure in terms of proton and nucleon distributions in Ru and Zr will make a difference in the cross section.

In Fig. 1, we present the P_{T}^{ee} distribution at 200 GeV in the Ru+Ru and Zr+Zr collisions. We observe that $d\sigma_{\text{Ru+Ru}}/dP_{\text{T}}^{\text{ee}}$ is always larger than $d\sigma_{\text{Zr+Zr}}/dP_{\text{T}}^{\text{ee}}$ due to different charges in Ru and Zr. The shapes of $d\sigma_{\text{Ru+Ru}}/dP_{\text{T}}^{\text{ee}}$ and $d\sigma_{\text{Zr+Zr}}/dP_{\text{T}}^{\text{ee}}$ are similar: the spectra have peaks at $P_{\text{T}}^{\text{ee}} \sim 45$ MeV and drop rapidly when $P_{\text{T}}^{\text{ee}} > 45$ MeV. We also show the ratio of $d\sigma_{\text{Ru+Ru}}/dP_{\text{T}}^{\text{ee}}$ to $d\sigma_{\text{Zr+Zr}}/dP_{\text{T}}^{\text{ee}}$. The ratio is expected to be $(Z_{\text{Ru}}/Z_{\text{Zr}})^4 = (44/40)^4$ but there

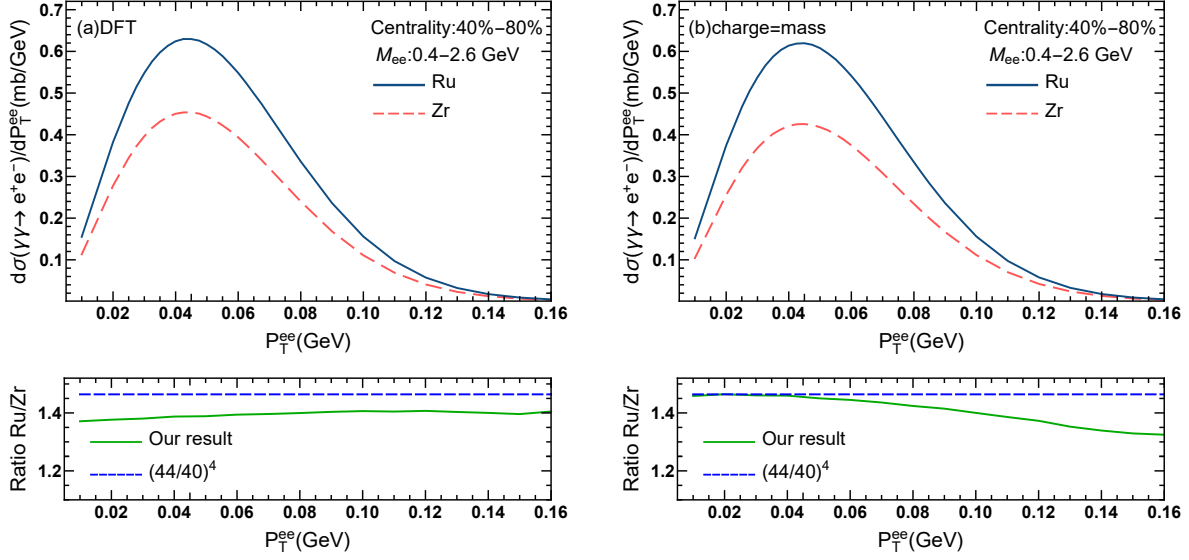


Figure 1. Differential cross sections in Ru+Ru and Zr+Zr collisions at 40-80% centrality as functions of P_T^{ee} . The subfigure (a) and (b) correspond to the set of parameters in Tab. I(a) and Tab. I(b) from the DFT calculation, respectively. In (b), we use the short-hand notation “charge=mass” for the case in Tab. I(b) in which the nuclear mass density distribution is chosen to be the same as the charge density distribution. In (a), the blue-solid and red-dashed lines are the results for Ru+Ru and Zr+Zr collisions, respectively. In (b), the green-solid line is the ratio of the differential cross section in Ru+Ru collisions to Zr+Zr collisions. The range of M_{ee} is set to $[0.4, 2.6]$ GeV.

is a little difference. As shown in Tab. I, such a difference is mainly due to the difference in impact parameters at given centralities and the nuclear charge form factors in Ru+Ru and Zr+Zr collisions. We see that the charge and mass distributions can lead to a difference between (a) and (b) in the range $P_T^{ee} \leq 40$ MeV. For case (a) [Fig. 1(a)] in which one distinguishes nuclear charge and mass density distributions, the ratio is always smaller than $(44/40)^4$, while for case (b) in which the nuclear mass density distribution is set to be equal to the charge density distribution, it is very close to $(44/40)^4$ at $P_T^{ee} \leq 40$ MeV. So the fine nuclear structure can affect the dilepton spectra and therefore can be directly measured in experiments. The ratio shown in Fig. 1(a) is one of our main prediction in this study.

We also calculate the ratio of $dN_{\text{Ru+Ru}}/dP_T^{ee}$ to $dN_{\text{Zr+Zr}}/dP_T^{ee}$ in Fig. 2, where the differ-

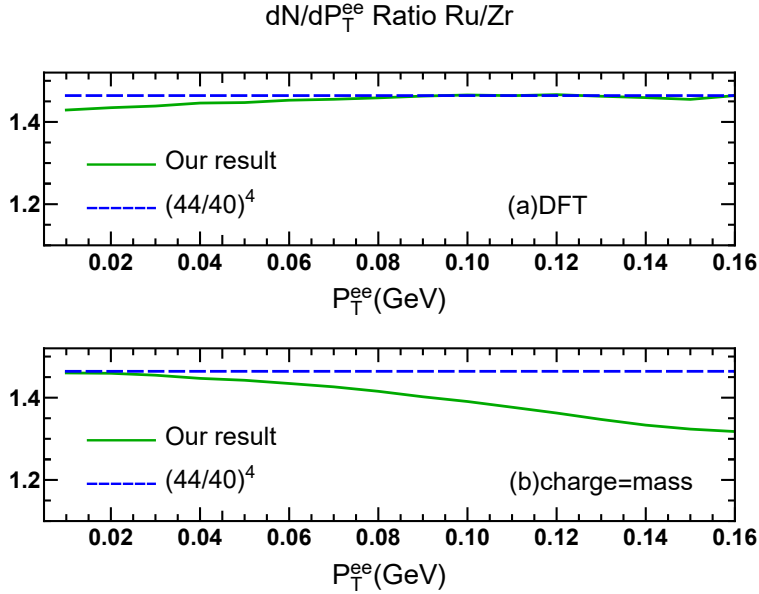


Figure 2. The ratio of dN/dP_T^{ee} in Ru+Ru to Zr+Zr collisions as functions of P_T^{ee} at 40-80% centrality. The definition of green-solid and blue-solid lines is the same as in Fig. 1.

ential yield dN is proportional to $d\sigma$ as

$$dN = \frac{d\sigma}{\pi(b_{T,\max}^2 - b_{T,\min}^2)}. \quad (5)$$

We observe that in case (a) the ratio of dN/dP_T^{ee} for Ru+Ru and Zr+Zr collisions is slightly smaller than $(44/40)^4$ at very small P_T^{ee} ($P_T^{ee} \leq 80$ MeV) by about 3%. The ratio in case (b) is similar to Fig. 1 (b).

The results for the differential cross sections as functions of the invariant mass of e^+e^- are shown in Fig. 3. The behavior of invariant mass spectra in Ru+Ru and Zr+Zr collisions is similar to Au+Au collisions [64, 65, 82, 91, 92]. The spectra have peaks at $M_{ee} \sim 0.5$ GeV and then decreases exponentially with increasing M_{ee} . In case (a) with the parameters in Tab. I(a), the ratio of $d\sigma_{\text{Ru+Ru}}/dM_{ee}$ to $d\sigma_{\text{Zr+Zr}}/dM_{ee}$ is always smaller than $(44/40)^4$, while the ratio in case (b) with the parameters in Tab. I(b) is almost equal to $(44/40)^4$.

The azimuthal angle distributions at 40-80% centrality in isobar collisions at 200 GeV are shown in Fig. 4. Our results show a modulation of $-\cos(4\phi)$ in Ru+Ru and Zr+Zr collisions with two sets of parameters in Tab. I. Such a modulation is related to the linear polarization of incident photons [85, 89, 92], see Refs. [93–98] for similar effects in QCD.

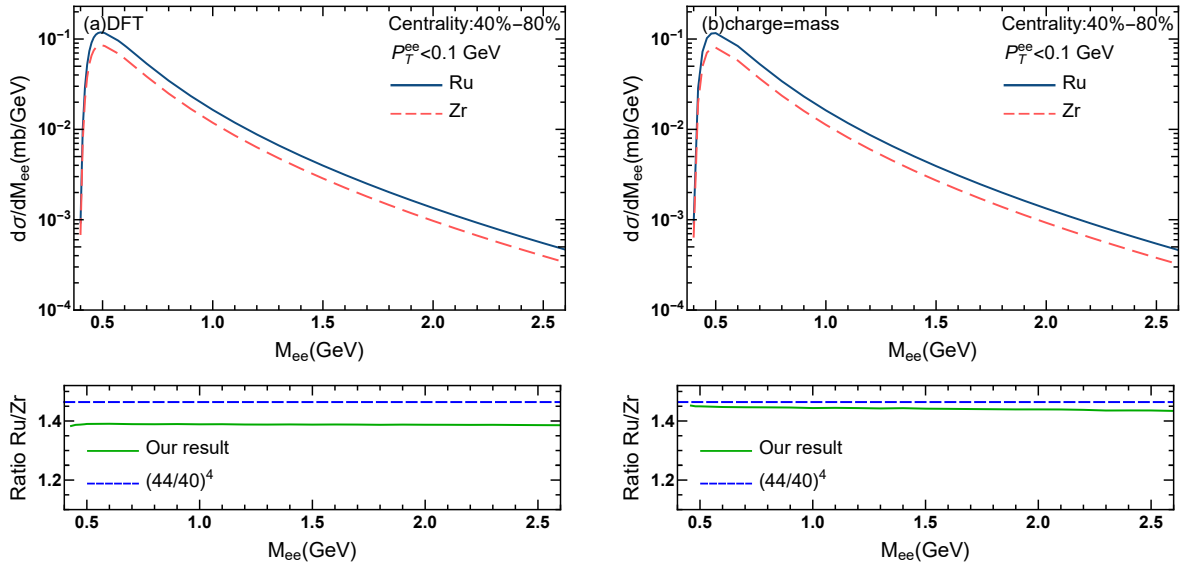


Figure 3. Differential cross sections of e^+e^- in 40-80% centrality as functions of M_{ee} . The parameters used in (a) and (b) are the same as in Fig. (1). The definition of color-dashed or color-solid lines are the same as Fig. (1). The range of P_T^{ee} is chosen as $P_T^{ee} < 0.1$ GeV.

The ratio of $d\sigma_{\text{Ru+Ru}}/d\phi$ to $d\sigma_{\text{Zr+Zr}}/d\phi$ is always smaller than $(44/40)^4$ in case (a), while it agrees with $(44/40)^4$ in case (b).

We see that the ratios of differential cross sections in Ru+Ru collisions to Zr+Zr collisions as functions of P_T^{ee} , M_{ee} and ϕ in case (a) are always smaller than $(44/40)^4$. So it provides a way of measuring the difference between the charge and mass distributions in isobar nuclei through P_T^{ee} , M_{ee} and ϕ spectra of lepton pairs in isobar collisions.

IV. CHARGE AND CENTRALITY DEPENDENCE

In this section, we study the charge and centrality dependence of cross sections in isobar collisions. We have presented the spectra of P_T^{ee} , M_{ee} and ϕ for di-electrons by using the set of parameters in case (a) and (b) in the previous section. In this section we will focus on case (a) in which the nuclear charge and mass density distributions are distinguished. In general, the deformation of colliding nuclei can have an effect on the spectra, but we do not consider it here and leave it for a future study.

In Fig. 5, we present the charge dependence of the integrated excess yield N scaled by

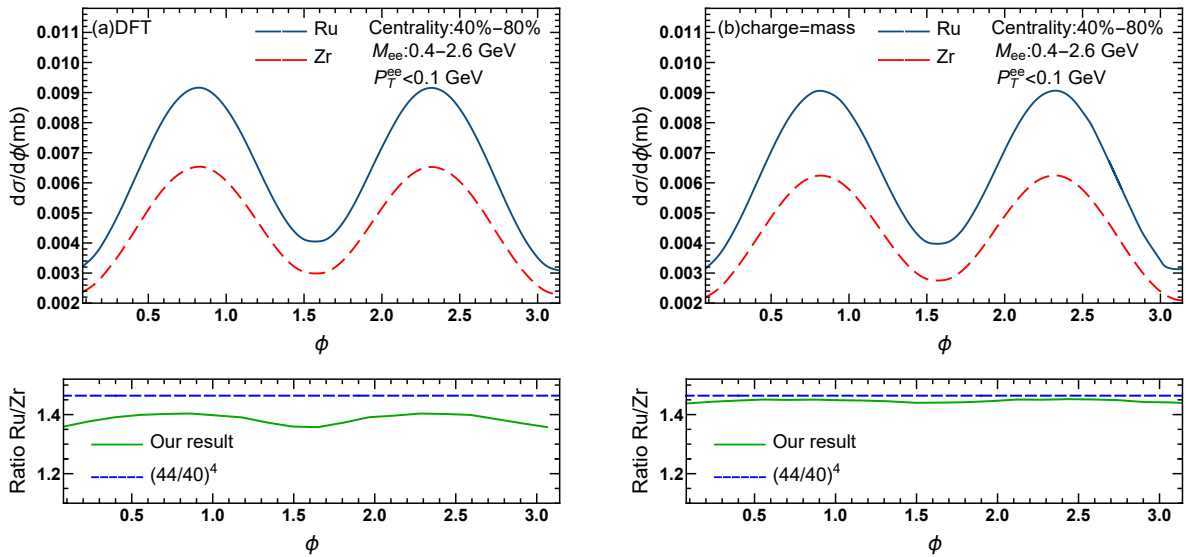


Figure 4. Differential cross sections in Ru+Ru and Zr+Zr collisions as functions of ϕ at 40-80% centrality. The definition of all color-solid and -dashed lines is the same as in Fig. 1. The ranges M_{ee} and P_T^{ee} are chosen as $M_{ee} \in [0.4, 2.6]$ GeV and $P_T^{ee} < 0.1$ GeV.

Z^4 , which is defined as the cross section in a specific range of impact parameters,

$$N = \frac{\int_{b_{T;\min}}^{b_{T;\max}} d\sigma}{\pi(b_{T;\max}^2 - b_{T;\min}^2)}. \quad (6)$$

The result shows that the integrated excess yield scaled by Z^4 decreases with Z , which is consistent with Ref.[65, 76]. Such a behavior is caused by different charge and mass distributions in different nuclei. For a given centrality, the ranges of impact parameters of different nuclei are different due to their mass distributions.

The centrality dependence of the integrated excess yield is summarized in Tab. II. We see that the ratio of the integrated excess yield in Ru+Ru collisions to Zr+Zr collisions is smaller than $(44/40)^4 \approx 1.4641$, which is consistent with the results in the previous section. The ratio increases slightly with the impact parameter.

In Fig. 6, we show $\sqrt{\langle (P_T^{ee})^2 \rangle}$ as functions of M_{ee} in 40-60% and 60-80% centrality ranges in Ru+Ru and Zr+Zr collisions. We see that $\sqrt{\langle (P_T^{ee})^2 \rangle}$ increases with increasing M_{ee} or decreasing impact parameters. The trend agrees with the previous work in Ref. [92] by some of us in Au+Au collisions. In contrast to $d\sigma/dP_T^{ee}$ in Fig. 1, $\sqrt{\langle (P_T^{ee})^2 \rangle}$ as functions of M_{ee} in Ru+Ru or Zr+Zr collisions are almost the same.

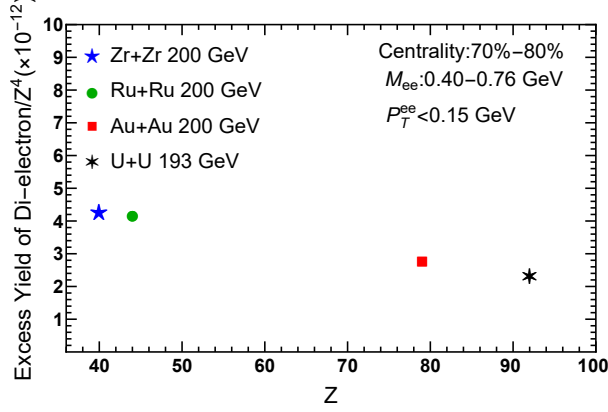


Figure 5. The charge dependence of the integrated excess yields scaled by Z^4 in 70-80% centrality in Ru+Ru, Zr+Zr, Au+Au and U+U collisions. The ranges of M_{ee} and P_T^{ee} are $M_{ee} \in [0.4, 0.76]$ GeV and $P_T^{ee} < 0.15$ GeV.

Table II. The centrality dependence of the integrated excess yield at 200 GeV in Ru+Ru and Zr+Zr collisions. The range of M_{ee} and P_T^{ee} are set to $M_{ee} \in [0.4, 2.6]$ GeV and $P_T^{ee} < 0.1$ GeV.

	Ru	Zr	ratio Ru/Zr
40-60%	2.328×10^{-5}	1.615×10^{-5}	1.441
60-70%	2.245×10^{-5}	1.549×10^{-5}	1.449
70-80%	2.178×10^{-5}	1.495×10^{-5}	1.457

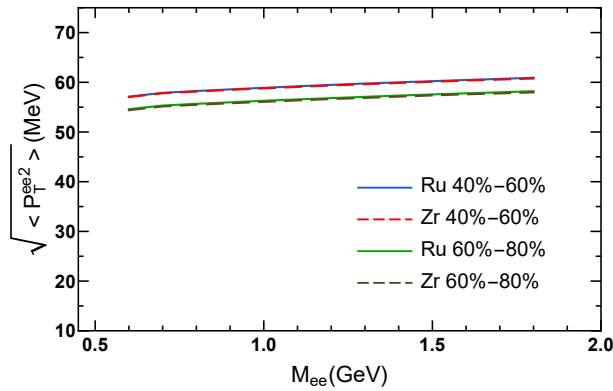


Figure 6. The average transverse momenta of di-electrons as functions of M_{ee} in 40-60% and 60-80% centrality ranges. The blue and green solid lines stand for 40-60% and 60-80% centralities in Ru+Ru collisions respectively. The red and brown dashed lines stand for the same centralities in Zr+Zr collisions respectively. We choose $P_T^{ee} < 0.1$ GeV.

V. CONCLUSION

We have investigated the photoproduction of di-electrons in peripheral isobar collisions based on the method developed in previous works by some of us [91, 92]. The nuclear mass and charge density distributions are described by Woods-Saxon distributions with the parameters determined from the DFT calculation. The charge density distribution gives the nuclear charge form factor in the photoproduction cross section for di-electrons. The centrality corresponds to the impact parameter in a Glauber model and is determined through the nuclear mass density distribution. According to the DFT, the nuclear mass density distribution is different from the nuclear charge density distribution in general. For comparison, we also consider the approximation that the mass density distribution is taken as equal to the charge density distribution.

We calculated the spectra of P_T^{ee} , M_{ee} and ϕ at 40-80% centrality in Ru+Ru and Zr+Zr collisions at 200 GeV. We take the ratio of these spectra in Ru+Ru collisions to Zr+Zr collisions. The results are presented in Fig. 1, Fig. 2, Fig. 3 and Fig. 4 which show the effect arising from the difference between the mass and charge density distributions. If one does not distinguish the charge and mass density distributions, these ratios are close to $(44/40)^4$, the ratio of the fourth power of the proton number. If one does distinguish them, these ratios are generally smaller than $(44/40)^4$ by a few percent. This is the main result of our paper.

We also calculated the charge and centrality dependence of integrated excess yield in isobar collisions. We find that it decreases with growing Z as shown in Fig. 5. Such a behavior reflects different charge and mass distributions in different nuclei. We present in Fig. 6 the spectra of $\sqrt{\langle(P_T^{ee})^2\rangle}$ as functions of M_{ee} in 40-60% and 60-80% centrality ranges in Ru+Ru and Zr+Zr collisions. The M_{ee} spectra of $\sqrt{\langle(P_T^{ee})^2\rangle}$ are found to be similar to Au+Au collisions [92] and is almost the same in Ru+Ru and Zr+Zr collisions.

With above results, we conclude that the photoproduction of lepton pairs in isobar collisions may provide a new way to probe the nuclear structure. We note that nuclear deformation effects are neglected in this paper and may have effects on above observables, which worths a future study.

ACKNOWLEDGMENTS

We would like to thank Fuqiang Wang, Xiao-Feng Wang, Bo-Wen Xiao and Jian Zhou for helpful discussion. This work is partly supported by National Natural Science Foundation of China (NSFC) under Grants No. 11909059, 12035006, 12075235, 12135011 and 12275082.

-
- [1] V. Skokov, A. Y. Illarionov, and V. Toneev, *Int. J. Mod. Phys. A* **24**, 5925 (2009), 0907.1396.
 - [2] A. Bzdak and V. Skokov, *Phys. Lett. B* **710**, 171 (2012), 1111.1949.
 - [3] W.-T. Deng and X.-G. Huang, *Phys. Rev. C* **85**, 044907 (2012), 1201.5108.
 - [4] V. Roy and S. Pu, *Phys. Rev. C* **92**, 064902 (2015), 1508.03761.
 - [5] S. Pu, V. Roy, L. Rezzolla, and D. H. Rischke, *Phys. Rev. D* **93**, 074022 (2016), 1602.04953.
 - [6] D. E. Kharzeev, L. D. McLerran, and H. J. Warringa, *Nucl. Phys. A* **803**, 227 (2008), 0711.0950.
 - [7] K. Fukushima, D. E. Kharzeev, and H. J. Warringa, *Phys. Rev. D* **78**, 074033 (2008), 0808.3382.
 - [8] X.-G. Huang and J. Liao, *Phys. Rev. Lett.* **110**, 232302 (2013), 1303.7192.
 - [9] S. Pu, S.-Y. Wu, and D.-L. Yang, *Phys. Rev. D* **89**, 085024 (2014), 1401.6972.
 - [10] S. Pu, S.-Y. Wu, and D.-L. Yang, *Phys. Rev. D* **91**, 025011 (2015), 1407.3168.
 - [11] J.-W. Chen, T. Ishii, S. Pu, and N. Yamamoto, *Phys. Rev. D* **93**, 125023 (2016), 1603.03620.
 - [12] Y. Hidaka, S. Pu, and D.-L. Yang, *Phys. Rev. D* **97**, 016004 (2018), 1710.00278.
 - [13] J.-H. Gao and Z.-T. Liang, *Phys. Rev. D* **100**, 056021 (2019), 1902.06510.
 - [14] N. Weickgenannt, X.-L. Sheng, E. Speranza, Q. Wang, and D. H. Rischke, *Phys. Rev. D* **100**, 056018 (2019), 1902.06513.
 - [15] N. Weickgenannt, E. Speranza, X.-l. Sheng, Q. Wang, and D. H. Rischke, *Phys. Rev. Lett.* **127**, 052301 (2021), 2005.01506.
 - [16] K. Hattori, Y. Hidaka, and D.-L. Yang, *Phys. Rev. D* **100**, 096011 (2019), 1903.01653.
 - [17] Z. Wang, X. Guo, S. Shi, and P. Zhuang, *Phys. Rev. D* **100**, 014015 (2019), 1903.03461.
 - [18] D.-L. Yang, K. Hattori, and Y. Hidaka, *JHEP* **07**, 070 (2020), 2002.02612.
 - [19] N. Weickgenannt, X.-L. Sheng, E. Speranza, Q. Wang, and D. H. Rischke, *Nucl. Phys. A* **1005**, 121963 (2021), 2001.11862.

- [20] S. Li and H.-U. Yee, Phys. Rev. D **100**, 056022 (2019), 1905.10463.
- [21] Y.-C. Liu, K. Mameda, and X.-G. Huang, Chin. Phys. C **44**, 094101 (2020), 2002.03753, [Erratum: Chin.Phys.C 45, 089001 (2021)].
- [22] N. Weickgenannt, E. Speranza, X.-l. Sheng, Q. Wang, and D. H. Rischke, Phys. Rev. D **104**, 016022 (2021), 2103.04896.
- [23] Z. Wang and P. Zhuang, (2021), 2105.00915.
- [24] X.-L. Sheng, N. Weickgenannt, E. Speranza, D. H. Rischke, and Q. Wang, Phys. Rev. D **104**, 016029 (2021), 2103.10636.
- [25] A. Huang *et al.*, Phys. Rev. D **103**, 056025 (2021), 2007.02858.
- [26] M. A. Stephanov and Y. Yin, Phys. Rev. Lett. **109**, 162001 (2012), 1207.0747.
- [27] D. T. Son and N. Yamamoto, Phys. Rev. D **87**, 085016 (2013), 1210.8158.
- [28] J.-H. Gao, Z.-T. Liang, S. Pu, Q. Wang, and X.-N. Wang, Phys. Rev. Lett. **109**, 232301 (2012), 1203.0725.
- [29] J.-W. Chen, S. Pu, Q. Wang, and X.-N. Wang, Phys. Rev. Lett. **110**, 262301 (2013), 1210.8312.
- [30] C. Manuel and J. M. Torres-Rincon, Phys. Rev. D **89**, 096002 (2014), 1312.1158.
- [31] C. Manuel and J. M. Torres-Rincon, Phys. Rev. D **90**, 076007 (2014), 1404.6409.
- [32] J.-Y. Chen, D. T. Son, M. A. Stephanov, H.-U. Yee, and Y. Yin, Phys. Rev. Lett. **113**, 182302 (2014), 1404.5963.
- [33] J.-Y. Chen, D. T. Son, and M. A. Stephanov, Phys. Rev. Lett. **115**, 021601 (2015), 1502.06966.
- [34] J.-W. Chen, J.-H. Gao, J. Liu, S. Pu, and Q. Wang, Phys. Rev. D **88**, 074003 (2013), 1305.1835.
- [35] Y. Hidaka, S. Pu, and D.-L. Yang, Phys. Rev. D **95**, 091901 (2017), 1612.04630.
- [36] N. Mueller and R. Venugopalan, Phys. Rev. D **97**, 051901 (2018), 1701.03331.
- [37] Y. Hidaka and D.-L. Yang, Phys. Rev. D **98**, 016012 (2018), 1801.08253.
- [38] Y. Hidaka, S. Pu, and D.-L. Yang, Nucl. Phys. A **982**, 547 (2019), 1807.05018.
- [39] J.-H. Gao, Z.-T. Liang, Q. Wang, and X.-N. Wang, Phys. Rev. D **98**, 036019 (2018), 1802.06216.
- [40] A. Huang, S. Shi, Y. Jiang, J. Liao, and P. Zhuang, Phys. Rev. D **98**, 036010 (2018), 1801.03640.

- [41] Y.-C. Liu, L.-L. Gao, K. Mameda, and X.-G. Huang, Phys. Rev. D **99**, 085014 (2019), 1812.10127.
- [42] S. Lin and A. Shukla, JHEP **06**, 060 (2019), 1901.01528.
- [43] S. Lin and L. Yang, Phys. Rev. D **101**, 034006 (2020), 1909.11514.
- [44] N. Yamamoto and D.-L. Yang, Astrophys. J. **895**, 56 (2020), 2002.11348.
- [45] Y. Hidaka, S. Pu, Q. Wang, and D.-L. Yang, (2022), 2201.07644.
- [46] S. Fang, S. Pu, and D.-L. Yang, (2022), 2204.11519.
- [47] J.-H. Gao, Z.-T. Liang, and Q. Wang, Phys. Rev. D **101**, 096015 (2020), 1910.11060.
- [48] J.-h. Gao, S. Pu, and Q. Wang, Phys. Rev. D **96**, 016002 (2017), 1704.00244.
- [49] X.-L. Luo and J.-H. Gao, JHEP **11**, 115 (2021), 2107.11709.
- [50] V. Roy, S. Pu, L. Rezzolla, and D. Rischke, Phys. Lett. B **750**, 45 (2015), 1506.06620.
- [51] I. Siddique, R.-j. Wang, S. Pu, and Q. Wang, Phys. Rev. D **99**, 114029 (2019), 1904.01807.
- [52] S. Shi, Y. Jiang, E. Lilleskov, and J. Liao, Annals Phys. **394**, 50 (2018), 1711.02496.
- [53] S. Pu and D.-L. Yang, Phys. Rev. D **93**, 054042 (2016), 1602.04954.
- [54] G. Inghirami *et al.*, Eur. Phys. J. C **76**, 659 (2016), 1609.03042.
- [55] D. E. Kharzeev, J. Liao, S. A. Voloshin, and G. Wang, Prog. Part. Nucl. Phys. **88**, 1 (2016), 1511.04050.
- [56] J. Liao, Pramana **84**, 901 (2015), 1401.2500.
- [57] V. A. Miransky and I. A. Shovkovy, Phys. Rept. **576**, 1 (2015), 1503.00732.
- [58] X.-G. Huang, Rept. Prog. Phys. **79**, 076302 (2016), 1509.04073.
- [59] K. Fukushima, Prog. Part. Nucl. Phys. **107**, 167 (2019), 1812.08886.
- [60] A. Bzdak *et al.*, Phys. Rept. **853**, 1 (2020), 1906.00936.
- [61] J. Zhao and F. Wang, Prog. Part. Nucl. Phys. **107**, 200 (2019), 1906.11413.
- [62] J.-H. Gao, G.-L. Ma, S. Pu, and Q. Wang, Nucl. Sci. Tech. **31**, 90 (2020), 2005.10432.
- [63] ATLAS, M. Aaboud *et al.*, Nature Phys. **13**, 852 (2017), 1702.01625.
- [64] STAR, J. Adam *et al.*, Phys. Rev. Lett. **127**, 052302 (2021), 1910.12400.
- [65] W. Zha, J. D. Brandenburg, Z. Tang, and Z. Xu, Phys. Lett. B **800**, 135089 (2020), 1812.02820.
- [66] K. Hattori and K. Itakura, Annals Phys. **330**, 23 (2013), 1209.2663.
- [67] K. Hattori and K. Itakura, Annals Phys. **334**, 58 (2013), 1212.1897.
- [68] K. Hattori, H. Taya, and S. Yoshida, JHEP **01**, 093 (2021), 2010.13492.

- [69] K. Hattori and K. Itakura, (2022), 2205.04312.
- [70] S. L. Adler, *Annals Phys.* **67**, 599 (1971).
- [71] J. S. Schwinger, *Phys. Rev.* **82**, 664 (1951).
- [72] P. Copinger, K. Fukushima, and S. Pu, *Phys. Rev. Lett.* **121**, 261602 (2018), 1807.04416.
- [73] P. Copinger and S. Pu, *Int. J. Mod. Phys. A* **35**, 2030015 (2020), 2008.03635.
- [74] P. Copinger and S. Pu, *Phys. Rev. D* **105**, 116014 (2022), 2203.00847.
- [75] ATLAS, M. Aaboud *et al.*, *Phys. Rev. Lett.* **121**, 212301 (2018), 1806.08708.
- [76] STAR, J. Adam *et al.*, *Phys. Rev. Lett.* **121**, 132301 (2018), 1806.02295.
- [77] ALICE, (2022), 2204.11732.
- [78] S. R. Klein, J. Nystrand, J. Seger, Y. Gorbunov, and J. Butterworth, *Comput. Phys. Commun.* **212**, 258 (2017), 1607.03838.
- [79] M. Vidovic, M. Greiner, C. Best, and G. Soff, *Phys. Rev. C* **47**, 2308 (1993).
- [80] K. Hencken, D. Trautmann, and G. Baur, *Phys. Rev. A* **51**, 1874 (1995), nucl-th/9410014.
- [81] K. Hencken, G. Baur, and D. Trautmann, *Phys. Rev. C* **69**, 054902 (2004), nucl-th/0402061.
- [82] W. Zha, L. Ruan, Z. Tang, Z. Xu, and S. Yang, *Phys. Lett. B* **781**, 182 (2018), 1804.01813.
- [83] J. D. Brandenburg *et al.*, (2020), 2006.07365.
- [84] J. D. Brandenburg, W. Zha, and Z. Xu, *Eur. Phys. J. A* **57**, 299 (2021), 2103.16623.
- [85] C. Li, J. Zhou, and Y.-J. Zhou, *Phys. Rev. D* **101**, 034015 (2020), 1911.00237.
- [86] X. Wang *et al.*, (2022), 2207.05595.
- [87] S. Klein, A. H. Mueller, B.-W. Xiao, and F. Yuan, *Phys. Rev. Lett.* **122**, 132301 (2019), 1811.05519.
- [88] S. Klein, A. H. Mueller, B.-W. Xiao, and F. Yuan, *Phys. Rev. D* **102**, 094013 (2020), 2003.02947.
- [89] C. Li, J. Zhou, and Y.-J. Zhou, *Phys. Lett. B* **795**, 576 (2019), 1903.10084.
- [90] B.-W. Xiao, F. Yuan, and J. Zhou, *Phys. Rev. Lett.* **125**, 232301 (2020), 2003.06352.
- [91] R.-j. Wang, S. Pu, and Q. Wang, *Phys. Rev. D* **104**, 056011 (2021), 2106.05462.
- [92] R.-j. Wang, S. Lin, S. Pu, Y.-f. Zhang, and Q. Wang, (2022), 2204.02761.
- [93] E. Akcakaya, A. Schäfer, and J. Zhou, *Phys. Rev. D* **87**, 054010 (2013), 1208.4965.
- [94] A. Schafer and J. Zhou, *Phys. Rev. D* **85**, 114004 (2012), 1203.1534.
- [95] D. Boer, P. J. Mulders, J. Zhou, and Y.-j. Zhou, *JHEP* **10**, 196 (2017), 1702.08195.
- [96] F. Dominguez, J.-W. Qiu, B.-W. Xiao, and F. Yuan, *Phys. Rev. D* **85**, 045003 (2012),

1109.6293.

- [97] A. Metz and J. Zhou, Phys. Rev. D **84**, 051503 (2011), 1105.1991.
- [98] Y. Hagiwara, C. Zhang, J. Zhou, and Y.-j. Zhou, (2021), 2106.13466.
- [99] H. Xing, C. Zhang, J. Zhou, and Y.-J. Zhou, JHEP **10**, 064 (2020), 2006.06206.
- [100] STAR, M. Abdallah *et al.*, (2022), 2204.01625.
- [101] STAR, M. Abdallah *et al.*, Phys. Rev. Lett. **128**, 122303 (2022), 2109.07625.
- [102] J. D. Brandenburg *et al.*, (2022), 2207.02478.
- [103] S. A. Voloshin, Phys. Rev. Lett. **105**, 172301 (2010), 1006.1020.
- [104] H.-J. Xu *et al.*, Phys. Rev. Lett. **121**, 022301 (2018), 1710.03086.
- [105] H. Li *et al.*, Phys. Rev. C **98**, 054907 (2018), 1808.06711.
- [106] STAR, M. Abdallah *et al.*, Phys. Rev. C **105**, 014901 (2022), 2109.00131.
- [107] STAR, J. Zhou, EPJ Web Conf. **259**, 13014 (2022).
- [108] H.-j. Xu *et al.*, Phys. Rev. C **105**, L011901 (2022), 2105.04052.
- [109] H.-j. Xu, H. Li, X. Wang, C. Shen, and F. Wang, Phys. Lett. B **819**, 136453 (2021), 2103.05595.
- [110] W.-T. Deng, X.-G. Huang, G.-L. Ma, and G. Wang, Phys. Rev. C **94**, 041901 (2016), 1607.04697.
- [111] M. L. Miller, K. Reygers, S. J. Sanders, and P. Steinberg, Ann. Rev. Nucl. Part. Sci. **57**, 205 (2007), nucl-ex/0701025.
- [112] C. Zhang and J. Jia, Phys. Rev. Lett. **128**, 022301 (2022), 2109.01631.
- [113] H.-Z. Wu, J.-J. Zhang, L.-G. Pang, and Q. Wang, Comput. Phys. Commun. **248**, 106962 (2020), 1902.07916.
- [114] J.-J. Zhang and H.-Z. Wu, Comput. Phys. Commun. **251**, 107240 (2020), 1910.01965.
- [115] J.-J. Zhang, H.-Z. Wu, S. Pu, G.-Y. Qin, and Q. Wang, Phys. Rev. D **102**, 074011 (2020), 1912.04457.
- [116] J.-J. Zhang *et al.*, (2022), 2201.06171.